IEEE Access
Multidisciplinary | Rapid Review | Open Access Journal

Received August 7, 2019, accepted August 22, 2019, date of publication September 3, 2019, date of current version September 17, 2019.

Digital Object Identifier 10.1109/ACCESS.2019.2939229

A Global Optimization Method for Specular Highlight Removal From a Single Image

WENYAO XIA[1,2], ELVIS C. S. CHEN[1,2], STEPHEN E. PAUTLER[3], AND TERRY M. PETERS[1,2], (Fellow, IEEE)

[1]Robarts Research Institute, Western University, London, ON N6A 3K7, Canada
[2]Department of Medical Biophysics, Medical Imaging, School of Biomedical Engineering, Western University, London, ON N6A 3K7, Canada
[3]Departments of Surgery and Oncology, Western University, London, ON N6A 3K7, Canada

Corresponding author: Wenyao Xia (wenyao_x@yahoo.ca)

This work was supported in part by the Canadian Institutes for Health Research under Grant FDN 201409, in part by the Canadian Foundation for Innovation under Grant LEF 20994, in part by the Natural Sciences and Engineering Research Council of Canada under Grant RGPIN 2014 04504, and in part by the Ontario Graduate Scholarship.

ABSTRACT The presence of specular highlight is a critical issue for both natural and medical images such as those produced by laparoscopes, which can lead to erroneous visual tracking, stereo reconstruction, and image segmentation. Specular highlight removal from a single image is necessary for image analysis and applications. Due to the differences between natural and medical image scenes, existing literature to address this issue has only been effective on natural images or medical images with textureless regions. To overcome this limitation, we propose a global optimization method for specular highlight removal from a single image based on a dichromatic reflection model. In addition to introducing modified illumination chromaticity, the proposed method consists of two novel steps: one for estimating diffuse chromaticity by correcting hue and saturation on highlighted regions, and the other for estimating diffuse and specular reflection coefficients using convex optimization with double regularization. The estimated diffuse chromaticity is proven to approximate the true diffuse chromaticity and the proposed optimization algorithm is guaranteed to find the optimal diffuse coefficients. Experimental results show that the proposed method can effectively remove specular highlights from both natural images and endoscopic images with texture detail preservation. To further demonstrate the efficacy of our proposed method, an application of stereo reconstruction using a public dataset illustrates that our highlight removal method can enhance surface reconstruction accuracy from 1.10mm RMSD to 0.69mm RMSD.

INDEX TERMS Specular reflection separation, highlight removal, diffuse chromaticity estimation, convex optimization, natural image, endoscopic image.

I. INTRODUCTION

Digital images captured under discrete source illumination often contain specular reflections, which conceal useful image features such as colors and textures [1], [2]. Aside from natural images, the presence of specular highlights following the advancement of minimally invasive surgeries also becomes an important issue for endoscopic images. Minimally invasive surgery is performed through small incisions by using small tubes and cameras, leading to less trauma to the body than the traditional open surgery [3], [4]. Due to the proximity of the camera light source and organ surfaces, endoscopic images often suffer from strong specular highlights, which can both negatively affect the visual quality and degrade the subsequent tasks of computer vision algorithms, such as visual tracking, stereo reconstruction, and image segmentation [5], [6]. In addition, regions with specular highlights may contain vital information relating to the organ such as color and textures. Therefore, it is desirable to remove specular reflections while preserving the original color and texture details of the organ surface for medical imaging applications. Numerous highlight removal methods have been presented in the literature. They can be categorized into multi-and single-image methods. The multi-image method employs different light information from a group of images. For example, Wang *et al.* [22] proposed a energy minimization with respect to the local weighting coefficient for highlight removal from multiple images, based

The associate editor coordinating the review of this article and approving it for publication was Shiqi Wang.

on a polarization filter. Shah *et al.* [17] proposed a specular highlight removal method from image sequences by using feature corresponding points. For a detailed survey on highlight removal methods, the reader may refer to [2] and the references therein. This paper focuses on specular reflection removal from a single color image.

In contrast, the single-image method separates the reflection component using a single image only. In addition to conventional color histogram analysis [47], categorically they can be classified into dichromatic reflection model-based [9]–[21], [23], [42]–[46], inpainting-based [24]–[29] and learning-based methods [30]–[32]. Since the dichromatic reflection model was introduced by Shafer [9], many model-based methods have been presented. These methods were reported to be effective on natural images, but less so on medical images, since some assumptions made for natural images are not valid in a medical context such as endoscopy. In contrast, the inpainting-based method used in medical imaging mainly includes both highlight detection and inpainting correction. The inpainting-based method provides visually pleasing and coherent images when highlight regions are very small, yet their texture details in the inpainted specular highlight region are often lost, due to neighborhood interpolation limitation. In recent years, deep learning-based methods have become popular in the computer vision and medical imaging community. The learning-based method usually requires a good training set to be available and thus is not generalizable for different image scenes. Therefore, developing an accurate and efficient method for removing specular highlights from a single image with texture detail preservation remains a challenging issue.

In this paper, we propose a global optimization method for specular highlight removal from a single image. The proposed method consists of modified illumination chromaticity and two novel steps: one for estimating diffuse chromaticity by correcting hue and saturation on highlighted regions, and another for estimating diffuse and specular reflection coefficients using convex optimization with double regularization. Experimental results demonstrate that the proposed method is more effective at removing specular highlights from both nature images and medical images, while preserving texture details. Finally, an application example for stereo reconstruction further illustrates that the proposed method can be useful for enhancing surface reconstruction accuracy from 1.10mm RMSD to 0.69mm RMSD. The contributions of this paper are four-fold:

- A modified illumination chromaticity with parameter perturbation is introduced to solve the problem of illumination chromaticity on fully saturated highlight images.
- A new diffuse chromaticity estimate is proposed by a joint RGB-space and HSV-space detection set, and an adaptive inpainting technique.
- Theoretical analysis proves that the estimated diffuse chromaticity can approximate the true diffuse chromaticity.
- A double gradient regularization-based convex optimization method for reflection coefficients is presented, and an iteration algorithm is guaranteed to find the optimal reflection coefficients.

The paper is organized as follows. Section II briefly reviews related work of single-image methods for specular highlight removal, while Section III introduces the proposed method. Section IV gives performance analysis and algorithm implementation, and Section V reports the experimental results. Finally, the conclusion and discussion are presented in Section VI.

II. RELATED WORK

Single-image methods for highlight removal can be divided into three main categories: dichromatic reflection model-based, inpainting-based, and learning-based methods.

A. DICHROMATIC REFLECTION MODEL-BASED METHODS

The dichromatic reflection model [9] is widely used for studying reflection components of a natural color image, whose intensity $I(\mathbf{x})$ at pixel $\mathbf{x} = (x, y)$ can be described as the combination of diffuse reflection $I_D(\mathbf{x})$ and specular reflection $I_S(\mathbf{x})$:

$$I(\mathbf{x}) = I_D(\mathbf{x}) + I_S(\mathbf{x}) = m_d(\mathbf{x})\Lambda(\mathbf{x}) + m_s(\mathbf{x})\Gamma(\mathbf{x}), \quad (1)$$

where $\Lambda(\mathbf{x})$ and $\Gamma(\mathbf{x})$ are the chromaticity of the diffuse reflection and illumination (specular) reflection and $m_d(\mathbf{x})$ and $m_s(\mathbf{x})$ are the diffuse and specular reflection coefficients (parameters), respectively. In RGB color space, $I(\mathbf{x}) = [I_r(\mathbf{x}), I_g(\mathbf{x}), I_b(\mathbf{x})]^T$ is the color intensity vector at pixel $\mathbf{x}$, $\Lambda(\mathbf{x}) = [\Lambda_r(\mathbf{x}), \Lambda_g(\mathbf{x}), \Lambda_b(\mathbf{x})]^T$ is the diffuse chromaticity vector, and $\Gamma(\mathbf{x}) = [\Gamma_r(\mathbf{x}), \Gamma_g(\mathbf{x}), \Gamma_b(\mathbf{x})]^T$ is the illumination chromaticity vector. The goal of specular highlight removal is to obtain a specular-free image estimate, based on received highlight image $I(\mathbf{x})$. Because both diffuse chromaticity and reflection coefficients are unknown, specular highlight removal is an ill-posed and blind separation problem.

Many dichromatic reflection model-based methods have been reported to be effective on natural images [9]–[23]. Considerable efforts were devoted to non-optimization modeling techniques, including pseudo specular-free image, color clustering, bilateral filter, and intensity ratio, respectively. In particular, by introducing a pseudo specular-free image Tan and Ikeuchi [14] proposed a highlight removal method without explicit color segmentation, based on diffuse pixel identification and chromaticity analysis [13]. Yang et al. [23] presented a robust diffuse chromaticity estimation method by applying a low-pass filter. To enhance computation speed, Shen and Cai [15] approximated the chromaticity of diffuse reflection using the pseudo specular-free image. By choosing a proper chromaticity threshold, Shen and Zheng [10] proposed a intensity ratio-based highlight removal method with color clustering so that the specular components can be easily computed. By using a bilateral filter, Yang *et al.* [11] proposed a specular highlight removal method under appropriate bilateral filter parameters. Suo *et al.* [8] proposed an effective highlight removal method, by introducing adaptive

color clustering so that diffuse components can be recovered quickly. By using color clustering, Ren *et al.* [12] proposed a highlight removal method with color-line constraint so that the specular and diffuse components can be computed fast. Recently, for an effective application to ocean surface remote sensing images, Wang *et al.* [44] proposed a highlight removal method by modifying Shen's method. To further improve Shen's method, dos Santos Souza *et al.* [45] proposed an improved clustering algorithm in the maximum and minimum chromaticity space derived from a pseudo specular free image, and then separate diffuse and specular components by an adaptive intensity ratio estimate.

Optimization modeling-based methods for specular highlight removal from natural images have been developed in recent years. Most of them are based on the variation of the dichromatic reflection model:

$$\hat{I}(\mathbf{x}) = \alpha(\mathbf{x})\Lambda(\mathbf{x}) + (1 - \alpha(\mathbf{x}))\Gamma(\mathbf{x})$$

where

$$\hat{I}(\mathbf{x}) = \frac{I(\mathbf{x})}{\Sigma_{c\in\{r,g,b\}} I_c(\mathbf{x})}, \quad \alpha(\mathbf{x}) = \frac{m_d(\mathbf{x})}{m_d(\mathbf{x}) + m_s(\mathbf{x})}.$$

In particular, Zhao *et al.* [20] proposed solving the following optimization problem:

$$\min_{(\alpha,\Lambda)} \sum_x f_1(\alpha(\mathbf{x}), \Lambda(\mathbf{x})) + \beta_1 f_2(\Lambda(\mathbf{x})) + \beta_2 f_3(\alpha(\mathbf{x}), \Lambda(\mathbf{x})) \tag{2}$$

where $f_1 = \|\hat{I}(\mathbf{x}) - \alpha(\mathbf{x})\Lambda(\mathbf{x}) - (1 - \alpha(\mathbf{x}))\Gamma(\mathbf{x})\|_2^2$, $f_2 = \sum_{\mathbf{z}} w(\mathbf{x}, \mathbf{z})\|\Lambda(\mathbf{x}) - \Lambda(\mathbf{z})\|_2^2$, and f_3 is the structure similarity function. Kim *et al.* [21] solved the following problem:

$$\min_{(\alpha,\Lambda,\lambda)} \sum_x f_1(\alpha(\mathbf{x}), \Lambda(\mathbf{x})) + \beta_1 \|\nabla(1 - \alpha(\mathbf{x}))\|_2 + \|\nabla\Lambda_\lambda(\mathbf{x}))\|_1 + \beta_2\|\lambda(\mathbf{x})\|_0 \tag{3}$$

where $\|\cdot\|_0$ denote l_0 norm. Akashi and Okatani [42] proposed a method for separating reflection components based on a sparse non-negative matrix factorization optimization method, where the estimation of diffuse colors and the separation of reflection components was performed. Li *et al.* [43] introduced a modified reflection model for facial skin images. Based on the reflection model, an optimization method for the diffuse and specular components was presented, where the objective function contains a data term as well as two regularization, isotropic and anisotropic smoothness terms. Wei *et al.* [18] presented an optimization method for specular highlight reduction by assuming that the surface geometry is known. These methods may estimate simultaneously diffuse and and specular reflection. Yet, because of the non-convexity of the associated objective function in these methods, an alternating direction algorithm is in general employed, and thus proper initial points are required due to local minima problem. For robustness to outliers, Guo *et al.* [46] proposed a highlight removal method by solving the following nuclear-norm and l_1-norm optimization problem:

$$\min_{(W_d,\Gamma,M_s)} \|W_d\|_* + \lambda\|M_s\|_1 + \tau\|W_d\|_1 \quad Y = \Phi_d W_d + \Gamma M_s, \quad W_d \geq O,\ M_s \geq O \tag{4}$$

where $\|\cdot\|_*$ denotes the nuclear norm, Y is an observed color matrix, Φ_d is a color dictionary matrix, W_d is a matrix of weighting coefficients of pixels, Γ is a column vector of illumination chromaticity, and M_s is a row vector of specular highlights. Under the condition of a given color dictionary matrix, an alternating iteration scheme is presented by using an augmented Lagrange function to solve (4).

B. INPAINTING-BASED METHODS

The inpainting-based method includes two main steps [6]. The first is to detect image highlights in each frame, based on various color spaces such as RGB, YUV, HSV, and HSI, respectively. The second is to correct the highlight pixels by using spatial and temporal pixel interpolation. Tan *et al.* [24] first introduced an inpainting method for highlight removal. Thereafter, joint detection and inpainting-based methods were presented in [24]–[29], [33], [34]. Oh *et al.* [33] proposed one HSV space-based method for detecting specular highlights by using two threshold sets:

$$S(\mathbf{x}) < T_s, \quad V(\mathbf{x}) > T_v. \tag{5}$$

where the highlight image was segmented into two areas, absolute and relative bright areas. Naturally, the detection method is effective but the detected relative bright areas may include white surfaces. Stehle [26] used a inpainting technique with texture filling, while Meslouhi *et al.* [28] employed a reflection enhancement technique to improve highlight detection accuracy, and an inpainting-based algorithm for specular reflection removal in colposcopic images. Saint-Pierre *et al.* [29] presented an inpainting technique to correct specular reflections in thoracoscopic images. Arnold *et al.* [27] proposed a RGB space-based detection method, while Bernal *et al.* [34] proposed an modified RGB space-based method to enhance specular highlight detection. These inpainting-based methods are only effective on endoscopic images with very small highlight regions. In other cases, the texture details in the inpainted region are often lost due to neighborhood interpolation limitations.

C. LEARNING-BASED METHODS

Machine Learning approaches have been well used in image feature extraction, image classification, and image enhancement. Unlike both the dichromatic reflection model-based method and inpainting-based method, the learning-based method for highlight removal has no specular highlight model assumption, yet it needs a proper training set and time-consuming network training [30], [31]. Recently, Funke *et al.* [32] presented a generative adversarial network for specular highlight removal in endoscopic images. To train this network, small image patches with specular highlights and patches without highlights are extracted from endoscopic videos. As a result, this method was reported to be effective on small image patches with specular highlights. Nevertheless, this method exhibits image contrast and border artifact problems when integrating highlight-removed patches back to the complete image.

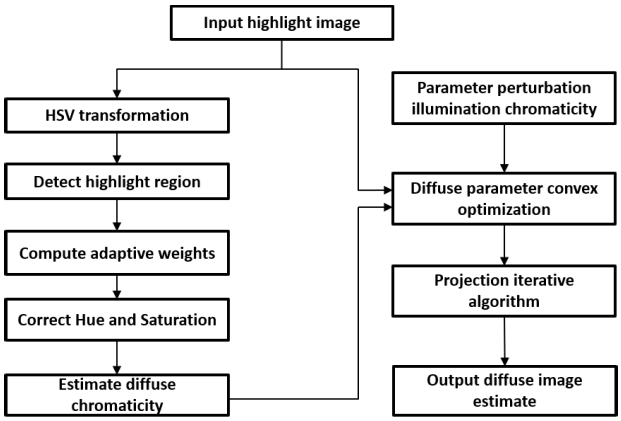

FIGURE 1. Scheme of proposed highlight removal method.

III. PROPOSED METHOD

To reduce the limitation of current highlight removal methods we propose a global optimization method for specular highlight removal from a single image based on the dichromatic model. First, we estimate the hue and saturation in HSV color space and obtain a diffuse chromaticity estimate by using the inverse transformation of HSV in RGB space. Second, using both the diffuse chromaticity estimate and modified illumination chromaticity, we minimize a double gradient regularization-based convex optimization problem to estimate diffuse reflection coefficients. Fig. 1 displays the workflow of our highlight removal method, which shows the relationship among various components that are discussed in subsequent subsections.

As an illustrative example, Fig. 2 displays highlight removal results of both natural and medical images by three methods, where Figs. 2 (a) and (e) are highlight images. Figs. 2(b) and (f) are results by using our method, (c) and (g) are results by using an inpainting-based method [29], and (d) and (h) are results by using a model based-method [12], where the specular free images are shown in the upper row and the separated specular

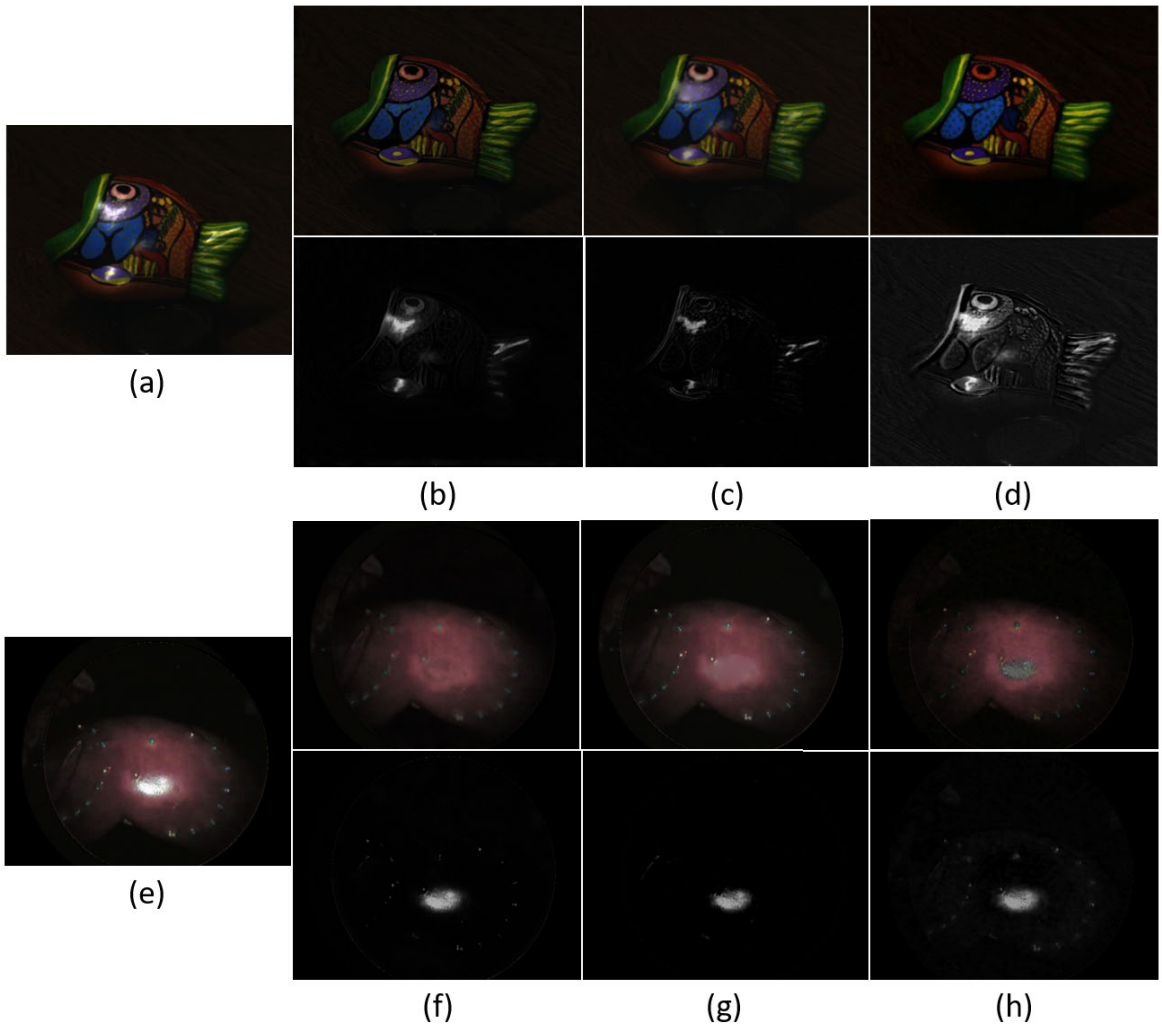

FIGURE 2. Highlight removal results of both natural and medical images. (a) and (e) input highlight images, (b) and (f) results by our method, (c) and (g) results by inpainting-based method [29], and (d) and (h) results by model based-method [12], where the specular free images are displayed in upper row and the separated specular components are shown in lower row.

TABLE 1. Comparison of characteristics of highlight removal methods.

Image	Method	Technique	Advantage	Requirement	Application scope	Speed	Refs.
Single image	Model-based non optimization	Pseudo diffuse image, local operation	No color segmentation	Diffuse pixel identification	Natural image	Fast	[14]
		Intensity ratio, color clustering	Effective specular reflection estimate	Chromaticity threshold	Natural image	Fast	[10],[15]
		Bilateral filter, pseudo diffuse image	Parallel computation, no color segmentation	Bilateral filter parameters	Natural image	Fast	[11]
		Orthogonal projection, pseudo diffuse image	Analytical diffuse reflection	Accurate color clustering	Natural image	Fast	[8]
		Color-line constraints, pseudo diffuse image	Analytical diffuse reflection	Accurate color clustering	Natural image	Fast	[12]
		Intensity ratio, GPU implementation	Improved pixel clustering	intensity ratio estimate	Natural image	Fast	[45]
	Model-based optimization	Non-convex optimization	Simultaneous diffuse and specular estimate	Alternating iteration, initial point choice	Natural image	Slow	[20],[21] [42],[43]
		Sparse and low-rank optimization	Robustness to strong Gaussian noise	Alternating iteration, proper color dictionary	Natural image	Slow	[46]
		Joint RGB and HSV space-based method, L2-L1 convex optimization	Reliable diffuse reflection estimate, no color distortion, global convergence	Projection iteration, proper color correction	Natural image, Endoscopic image	Slow	Our method
	Inpainting	Highlight detection, inpainting	No color distortion	Small highlight regions	Endoscopic image	Slow	[24-29], [33],[34]
	Deep learning	Image patch extracting, SpecGAN	Patch-based recovery	Proper network training	Endoscopic image	Slow	[32]
Multiple images	Polarization	Energy minimization, info. complementary	Removing highlights from polarized images	Polarization filter	Natural image	Slow	[22]
	Registration	Feature point matching, image fusion	Removing highlights of image sequences	Non-overlap highlights	Natural image	Fast	[17]

components are shown in the lower row. As shown in Figs. 2(c) and (g)(upper), the inpainting-based method cannot effectively remove highlights on the natural image and it loses the texture details in the inpainted region of the medical image. From Fig. 2(d)(upper) we observe that the model-based method is more effective on the nature image but Fig. 2(d)(lower) displays its incorrect specular components. From Fig. 2(h)(upper), it is seen that the model-based method is less effective on the medical images due to color distortion in the highlight region. In contrast, Figs. 2(b) and (f) show our highlight removal results. It is seen that our proposed method can effectively remove the highlight from both natural and medical images, while preserving the textures and color of the original scene.

Table 1 summarizes a comparison of the proposed method and current highlight removal methods in terms of technique characteristics and the scope of their application. Section IV shows the approximation of the estimated diffuse reflection and the global convergence of the proposed algorithm, respectively. Section V validates the effectiveness of the proposed method on specular highlight removal from a single natural image and endoscopic image with texture detail preservation.

A. MODIFIED ILLUMINATION CHROMATICITY

The current dichromatic reflection model-based methods are less effective on endoscopic images, since the illumination chromaticity is often assumed to be uniform for a given RGB image such that $\Gamma_r(\mathbf{x}) = \Gamma_g(\mathbf{x}) = \Gamma_b(\mathbf{x})$. Most of these approaches normalize the dichromatic reflection model by dividing the summation of its observed color image channels so that $\Gamma(\mathbf{x}) = [1/3, 1/3, 1/3]^T$ [10]. It is also common in the literature to have unnormalized $I(\mathbf{x})$ in the range $[0, 1]$, where $\Gamma(\mathbf{x}) = [1, 1, 1]^T$, and $0 \leq m_d(\mathbf{x}), m_s(\mathbf{x}) \leq 1$ [9]. However, because of the proximity of the light source to the organ surface, the specular highlights in endoscopic images are much stronger than those in natural images, such that some of the highlight pixels are saturated at maximum intensity. In other words, $\max\{I_r(\mathbf{x}), I_g(\mathbf{x}), I_b(\mathbf{x})\} = 1$.

Without the loss of generality, we consider unnormalized endoscopic images. Let X_0 denote the fully saturated highlight region. Then $I(\mathbf{x}) = [1, \eta, \theta]^T$ for any $\mathbf{x} \in X_0$ since $I_r(\mathbf{x}) \geq max\{I_g(\mathbf{x}), I_b(\mathbf{x})\}$, where $0 \leq \eta \leq 1$ and $0 \leq \theta \leq 1$. As a special case, $I(\mathbf{x}) = [1, 1, 1]^T$ for all $\mathbf{x} \in X_0$. From model (1) we thus have

$$(1 - m_s(\mathbf{x}))\Gamma(\mathbf{x}) = m_d(\mathbf{x})\Lambda(\mathbf{x}). \tag{6}$$

Since in vivo tissue is seldom pure white due to the presence of hemoglobin, the case that $\Lambda_r = \Lambda_g = \Lambda_b$ is mostly invalid for the endoscopic images. As a result, from $\Gamma(\mathbf{x}) = [1, 1, 1]^T$ or $\Gamma(\mathbf{x}) = [1/3, 1/3, 1/3]^T$ we get $m_d(\mathbf{x}) = 0$ for any $\mathbf{x} \in X_0$ and thus $I_D(\mathbf{x}) = m_d(\mathbf{x})\Lambda(\mathbf{x}) = 0$, which would force the restored specular-free image surface to contain a black hole on X_0.

To avoid the problem of conventional illumination chromaticity on the fully saturated specular reflection region in the endoscopic images, we introduce the following modified illumination chromaticity with parameter perturbation:

$$\Gamma_\epsilon(\mathbf{x}) = [1 - \epsilon, 1, 1]^T \tag{7}$$

where $1 > \epsilon > 0$. When the highlight region is very small, ϵ is chosen to be 0. Otherwise, ϵ is in general chosen as the mean intensity of the neighborhood around the highlight region.

B. SPECULAR HIGHLIGHT DETECTION AND COLOR CORRECTION

1) DESIGN OF HIGHLIGHT DETECTION SET

To detect specular highlights, we propose using two detection sets in RGB and HSV spaces, respectively. Using HSV transformation $\varphi(\cdot)$ [35], we convert the observed image $I(x)$ from RGB space to hue: $H(\mathbf{x})$, saturation: $S(\mathbf{x})$, and value $V(\mathbf{x})$. We introduce one threshold detection set in HSV space:

$$X_{SV}(\mathbf{x}) = \{\mathbf{x}|S(x) < \alpha, V(\mathbf{x}) > 1 - \alpha\} \tag{8}$$

Using the gradient magnitude of dark-channel image $\hat{I}(\mathbf{x}) = \min_{c\in\{r,g,b\}} I_c(\mathbf{x})$ we define another threshold detection set in RGB space:

$$X_G(\mathbf{x}) = \{\mathbf{x}|G(x) \geq \tau\} \tag{9}$$

where $\alpha > 0$, $\tau > 0$ are mainly two threshold values and $G(\mathbf{x}) = \frac{\sqrt{(\hat{I}(x+1,y)-\hat{I}(x-1,y))^2+(\hat{I}(x,y+1)-\hat{I}(x,y-1))^2}}{2}$.

Based on (8) and (9), we propose a joint HSV and RGB-space detection set as below:

$$X_{SVG}(\mathbf{x}) = X_{SV}(x) \bigcup X_G(\mathbf{x}). \tag{10}$$

2) CORRECTION OF HUE AND SATURATION

According to (10), we correct the hue and saturation of the observed image in HSV space.

For any $\mathbf{x} \in X_{SVG}(\mathbf{x})$, we correct the hue and saturation by using the adaptive inpainting update formulas below:

$$\mathbf{H}^*(x) = \frac{1}{\sum\limits_{u\in\Omega(\mathbf{x})} w_{SVG}(\mathbf{u})} \sum_{u\in\Omega(\mathbf{x})} \mathbf{H}(\mathbf{u}) w_{SVG}(u), \tag{11}$$

$$\mathbf{S}^*(x) = \frac{1}{\sum\limits_{u\in\Omega(\mathbf{x})} w_{HS}(\mathbf{x},\mathbf{u})} \sum_{u\in\Omega(\mathbf{x})} \mathbf{S}(\mathbf{u}) w_{HS}(\mathbf{x},\mathbf{u}) \tag{12}$$

where $\Omega(x)$ denotes a window at pixel x and two adaptive weights are defined as:

$$w_{SVG}(\mathbf{x}) = \begin{cases} \alpha, & \mathbf{x} \in X_{SVG}(\mathbf{x}) \\ 1, & else \end{cases} \tag{13}$$

$$w_{HS}(\mathbf{x},\mathbf{u}) = e^{\left(\frac{-(\mathbf{H}(\mathbf{x})-\mathbf{H}(\mathbf{u}))^2}{\sigma^2}\right)} e^{-(1-\mathbf{S}(\mathbf{u}))^2)} \tag{14}$$

where σ is the spread parameter commonly used in guided bilateral filters, which is often taken as 0.01 [14].

Remark 1: In general, the choice of window size $\Omega(x)$ affects the accuracy and computation of color inpainting for highlight removal. Taking a smaller window size may enhance the computation speed but reduce the accuracy of color inpainting, while a larger window size may improve the accuracy of color inpainting but increase computational cost. For a good balance between highlight removal quality and computational cost, we chose an optimal tradeoff window size. In Section V, by applying the proposed method with window sizes from 3×3 up till 11×11 to a natural image we observed that 7×7 is a relatively optimal window size.

C. DIFFUSE CHROMATICITY ESTIMATE

Let I_H^* and I_S^* be the corrected hue and saturation of an observed image $I(\mathbf{x})$ in HSV color space, respectively. The proposed diffuse chromaticity estimate is defined as

$$\Lambda^*(\mathbf{x}) = \varphi^{-1}(I_H^*, I_S^*, 1) \tag{15}$$

where $\varphi^{-1}(\cdot)$ is the inverse transformation from HSV color space to RGB color space.

D. CONVEX OPTIMIZATION FOR DIFFUSE REFLECTION

According to (15) and Theorem 1 in Section IV, we see that I_{DV} may be viewed as a diffuse coefficient. So, the nonlinear dichromatic reflection model (1) may be further rewritten as the following linear dichromatic reflection model:

$$I(\mathbf{x}) = m_d(\mathbf{x})\Lambda^*(\mathbf{x}) + m_s(\mathbf{x})\Gamma_\epsilon(\mathbf{x}) + \delta(\mathbf{x}) \tag{16}$$

where $\delta(\mathbf{x})$ is the model error.

To minimize the model error defined in (16), we minimize the data term:

$$E_1(m_d(\mathbf{x}), m_s(\mathbf{x})) = \frac{1}{2}\|m_d(\mathbf{x})\Lambda^*(\mathbf{x}) + m_s(\mathbf{x})\Gamma^* - I(\mathbf{x})\|_2^2 \tag{17}$$

where $\|\cdot\|_2$ denotes the l_2 norm and $\Gamma^* = \Gamma_\epsilon$. To overcome the ill-posed problem, we introduce double regularization. Because the specular-free image is smooth, its gradient changes slowly and thus we use one l_2-norm regularization term. The specular image mainly consists of large bright region and its gradient tends to be sparse, so we use another l_1-norm regularization term. Since the diffuse reflection and illumination chromaticity are given, we introduce the following double gradient regularization term:

$$E_2(m_d(\mathbf{x}), m_s(\mathbf{x})) = \beta_1\|\nabla m_d(\mathbf{x})\|_2^2 + \beta_2||\nabla m_s(\mathbf{x})||_1 \tag{18}$$

where $\|\cdot\|_1$ denotes l_1 norm, β_1 and β_2 are the regularization parameters, and $\nabla m_d(\mathbf{x})$, $\nabla m_s(\mathbf{x})$ are the gradient of $m_d(\mathbf{x})$, $m_s(\mathbf{x})$, respectively. Because the two gradient regularization terms can describe the smoothness and non-smoothness of diffuse and specular components, it is useful for texture detail preservation [36], [37].

By incorporating both (17) and (18), we propose a convex optimization method for diffuse reflection coefficients, which solves the following convex optimization problem:

$$\begin{aligned} &\min_{m_d,m_s} \sum_x = E_1(m_d(\mathbf{x}), m_s(\mathbf{x})) + E_2(m_d(\mathbf{x}), m_s(\mathbf{x})) \\ &s.t.\ 0 \leq m_d(\mathbf{x}) \leq 1, \quad 0 \leq m_s(\mathbf{x}) \leq 1 \end{aligned} \tag{19}$$

IV. PERFORMANCE ANALYSIS AND ALGORITHM IMPLEMENTATION

In this section, we analyze the performance of the proposed method and algorithm implementation.

A. PERFORMANCE ANALYSIS

As for the modified illumination chromaticity, we have the following property:

Proposition 1: Let the diffuse chromaticity $\Lambda(x)$ be converted into hue: $\Lambda_H(\mathbf{x})$, saturation: $\Lambda_S(\mathbf{x})$, and value $\Lambda_V(\mathbf{x})$ in HSV space. If $\Gamma_\epsilon(\mathbf{x})$ is taken in model (1) and $\Lambda_V(\mathbf{x}) = 1$, then $m_d(\mathbf{x}) > 0$ for any $\mathbf{x} \in X_0$.

Proof: See Appendix.

Remark 2: Proposition 1 shows that $\Gamma_\epsilon(\mathbf{x})$ can effectively handle the black hole problem in the saturated highlight regions. In addition, from the analysis of Proposition 1 we see that in the case that $I(\mathbf{x}) = [1, 1, 1]^T$ on the saturated highlight regions, Proposition 1 still holds for $\Gamma_\epsilon(\mathbf{x}) = [1, 1-\epsilon, 1]^T$ or $[1, 1, 1-\epsilon]^T$. However, in other cases that $I(\mathbf{x}) = [1, \eta, \theta]^T$ where $0 \le \eta < 1$ and $0 \le \theta < 1$, it is difficult for us to take a proper ϵ such that $m_d(\mathbf{x}) > 0$.

To analyze the approximation of the proposed diffuse chromaticity estimate, two useful properties of HSV transformation are first given as follows:

Proposition 2: Let $\varphi(\cdot)$ be an HSV transformation which converts an image in RGB color space to an image in HSV color space. Then for any free color value k

$$\varphi(kR, kG, kB) = (H, S, kV) \tag{20}$$

Proof: See Appendix.

Proposition 3: Let $\varphi^{-1}(\cdot)$ be an inverse transformation from HSV color space to RGB color space. Then

$$V\varphi^{-1}(H, S, 1) = \varphi^{-1}(H, S, V) \tag{21}$$

Proof: See Appendix.

Based on Propositions 2 and 3, we establish our main result that the estimated diffuse chromaticity can approximate true diffuse chromaticity:

Theorem 1: Let I_H^* and I_S^* be corrected hue and saturation respectively of the observed image $I(\mathbf{x})$ in HSV space, respectively. If $I_H^* \approx I_{DH}$ and $I_S^* \approx I_{DS}$ where I_{DH} and I_{DS} are hue and saturation elements of diffuse reflection in HSV space, respectively, then

$$I_{DV}\,\Lambda^*(\mathbf{x}) \approx m_d(\mathbf{x})\Lambda(\mathbf{x}) \tag{22}$$

where $\Lambda(\mathbf{x})$ is the diffuse chromaticity and $0 \le I_{DV} \le 1$ is the value element of diffuse reflection in HSV space.

Proof: See Appendix.

B. ALGORITHM IMPLEMENTATION

To implement the proposed optimization method, we first reformulate (19) based on the following Theorem:

Theorem 2: Solving (19) is equivalent to solving

$$\begin{cases} m_d(\mathbf{x}) = P_{\Omega_1}[m_d(\mathbf{x}) - \dfrac{\partial E}{\partial m_d}] \\ m_s(\mathbf{x}) = P_{\Omega_2}[m_s(\mathbf{x}) - \dfrac{\partial E}{\partial m_s}] \\ \mathbf{p}(\mathbf{x}) = P_{\Omega_3}[\mathbf{p}(\mathbf{x}) - \dfrac{\partial E}{\partial \mathbf{p}}], \quad \dfrac{\partial E}{\partial \mathbf{q}} = 0 \end{cases} \tag{23}$$

where $\mathbf{p} \in R^2$ and $\mathbf{q} \in R^2$ are Lagrange multiplier vectors, and $P_{\Omega_1}(\cdot)$, $P_{\Omega_2}(\cdot)$, $P_{\Omega_3}(\cdot)$ are the projection operators on sets $\Omega_1 = \{m_d |\ 0 \le m_d \le 1\}$, $\Omega_2 = \{m_s |\ 0 \le m_s \le 1\}$, and $\Omega_3 = \{\mathbf{p} = (p_1, p_2) \mid |p_i| \le 1\ (i = 1, 2)\}$, respectively, and

$$P_{\Omega_i}(z) = arg \min_{u \in \Omega_i} ||u - z||_2 \ (i = 1, 2, 3)$$

Proof: See in Appendix

Next, to compute the gradient in (23), we have

$$\frac{\partial E}{\partial \mathbf{p}} = \beta_2 \nabla m_s(\mathbf{x}), \quad \frac{\partial E}{\partial \mathbf{q}} = \beta_1(\nabla m_d(\mathbf{x}) - \mathbf{q}(\mathbf{x})).$$

On the other hand, by using the Gauss-Ostrogradsky theorem [7] we have

$$\mathbf{q}^T \nabla m_d(\mathbf{x}) = -m_d(\mathbf{x}) div(\mathbf{q}), \quad \mathbf{p}^T \nabla m_s(\mathbf{x}) = -m_s(\mathbf{x}) div(\mathbf{p}) \tag{24}$$

where $div(\mathbf{p}(\mathbf{x})) = \partial p_1(\mathbf{x})/\partial x + \partial p_2(\mathbf{x})/\partial y$ is the divergence of vector field $\mathbf{p}(\mathbf{x})$. Then

$$\frac{\partial E}{\partial m_d} = (m_d(\mathbf{x})\Lambda^*(\mathbf{x}) + m_s(\mathbf{x})\Gamma^* - I(\mathbf{x}))^T \Lambda^*(\mathbf{x}) - \beta_1 div(\mathbf{q}(\mathbf{x}))$$

and

$$\frac{\partial E}{\partial m_s} = (m_d(\mathbf{x})\Lambda^*(\mathbf{x}) + m_s(\mathbf{x})\Gamma^* - I(\mathbf{x}))^T \Gamma^* - \beta_2 div(\mathbf{p}(\mathbf{x})).$$

Combining the gradient representations above with (23), we introduce the following projection gradient algorithm for solving (19):

$$\begin{cases} m_d^{k+1}(\mathbf{x}) = P_{\Omega_1}[m_d^k(\mathbf{x}) - h_k \dfrac{\partial E}{\partial m_d}(m_d^k(\mathbf{x}), m_s^k(\mathbf{x}), \mathbf{q}^k(\mathbf{x}))] \\ m_s^{k+1}(\mathbf{x}) = P_{\Omega_2}[m_s^k(\mathbf{x}) - h_k \dfrac{\partial E}{\partial m_s}(m_d^k(\mathbf{x}), m_s^k(\mathbf{x}), \mathbf{p}^k(\mathbf{x}))] \\ \mathbf{p}^{k+1}(\mathbf{x}) = P_{\Omega_3}[\mathbf{p}^k(\mathbf{x}) - h_k \beta_2 \nabla m_s^k(\mathbf{x})] \\ \mathbf{q}^{k+1}(\mathbf{x}) = \mathbf{q}^k(\mathbf{x}) - h_k \beta_1 (\nabla m_d^k(\mathbf{x}) - \mathbf{q}^k(\mathbf{x})) \end{cases} \tag{25}$$

where $h_k > 0$ is the step length. According to the analysis given in [38], the projection iterative algorithm can converge globally to the optimal solution of (19) provided that the step length is appropriately small. Finally, a specular highlight removal algorithm is described in Algorithm 1.

Remark 3: There are two threshold and regularization parameters in Algorithm 1 and their choices may depend on the lighting conditions of the image scene. For endoscopic images with bright illumination, because the specular-free image region is smoother than the specular image region, the gradient of the specular-free image should be smaller than the gradient of the specular image. Thus the l_2-norm regularization term needs to be minimized. This implies that β_1 should be greater than β_2. On the other hand, α is the threshold value on the saturation layer. Since the fully saturated highlight region tends to be pure white, setting α to be small is helpful for its detection. Parameter τ is used to control the gradient magnitude of dark channel image. Since endoscopic images have brighter regions than the natural images, τ value for detecting endoscopic image should be greater than τ that employed for natural images.

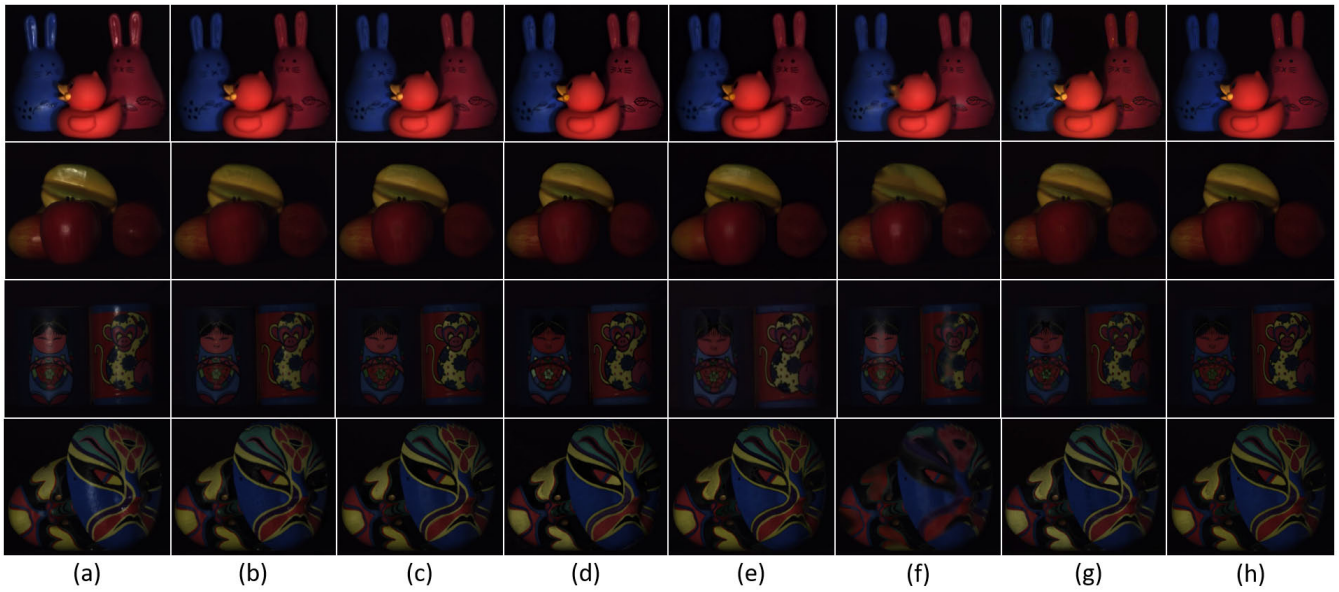

FIGURE 3. Highlight removal results for analytic natural images: (a) Highlight images, (b) Our method, (c) paper [10], (d) paper [12], (e) paper [11], (f) paper [34],(g) paper [8],(h) paper [45].

TABLE 2. Quantitative comparison of separation results.

Images	Masks		Cups		Fruit		Animals	
	PSNR	SSIM	PSNR	SSIM	PSNR	SSIM	PSNR	SSIM
[34]	23.75	0.79	33.15	0.94	33.73	0.96	32.36	0.98
[45]	34.90	0.95	39.50	0.97	39.40	**0.97**	37.50	0.97
[10]	34.12	0.91	39.20	0.96	38.90	0.97	37.25	0.98
[11]	32.20	0.92	37.63	0.95	37.54	0.97	36.46	0.97
[12]	34.54	0.93	38.01	0.96	37.75	0.97	36.89	0.98
[8]	34.20	0.93	37.27	0.95	**40.40**	0.97	35.26	0.96
Our method	**36.57**	**0.96**	**39.87**	**0.97**	39.98	0.96	**37.50**	**0.98**

Algorithm 1 For Specular Highlight Removal

1: Input: specular highlight image $I(\mathbf{x})$
2: Compute $\{H(\mathbf{x}), S(\mathbf{x}), V(\mathbf{x})\}$ by HSV transformation
3: Compute highlight detection sets by (8) and (9)
4: Compute Hue estimate $H^*(\mathbf{x})$ by (11)
5: Compute Saturation estimate $S^*(\mathbf{x})$ by (12)
6: Compute diffuse chromaticity estimate by (15)
7: Compute $m_d^*(\mathbf{x})$ by updating algorithm (25)
8: Compute $I_D^*(\mathbf{x}) = m_d^*(\mathbf{x})\Lambda^*(\mathbf{x})$
9: Output: Specular-free image estimate $I_D^*(\mathbf{x})$

V. EXPERIMENTS AND RESULTS

We evaluate the performance of the proposed method by testing natural and medical images. For natural images, we use the analytic and benchmark images which were used in previous studies [12]. For the medical images, we use the benchmark images from the well-known TMI dataset [41] and endoscopic images acquired from the local hospital. For specular highlight removal testing, we compare our method with five dichromatic reflection model-based methods: Shen's [10], Yang's [11], Suo's [8], Ren's [12], and Souza's [45] methods, and two inpainting-based methods: Saint-Pierre's [29] and Bernal's methods [34]. We perform the proposed algorithm on endoscopic images under design parameters $\alpha = 0.05$, $\beta_1 \in [1, 5]$, $\beta_2 = 0.1$, and $\tau \in [0.01, 0.1]$, and on natural images under design parameters $\alpha = 0.1$, $\tau = 0.01$, $\beta_1 = 3$, and $\beta_2 = 0.1$.

A. NATURAL IMAGE ASSESSMENT

1) ANALYTIC IMAGE TESTING

To analyze the proposed method quantitatively, we compare our method with the state-of-the art methods on four natural synthetic images (Masks, Cups, Fruit, and Animals) that have known ground truth. Figs. 3(b)-(g) demonstrate highlight removal results by using seven methods. From them we see that our results are visually similar to those of Shen and Zheng [10], Yang *et al.* [11], Suo *et al.* [8], Ren *et al.* [12], and Souza [45], and they are all better than Bernal's approach [34]. Furthermore, to quantify the highlight removal performance, we use the peak signal-to-noise ratio (PSNR) and structural similarity image measurement (SSIM) as objective measures [13].

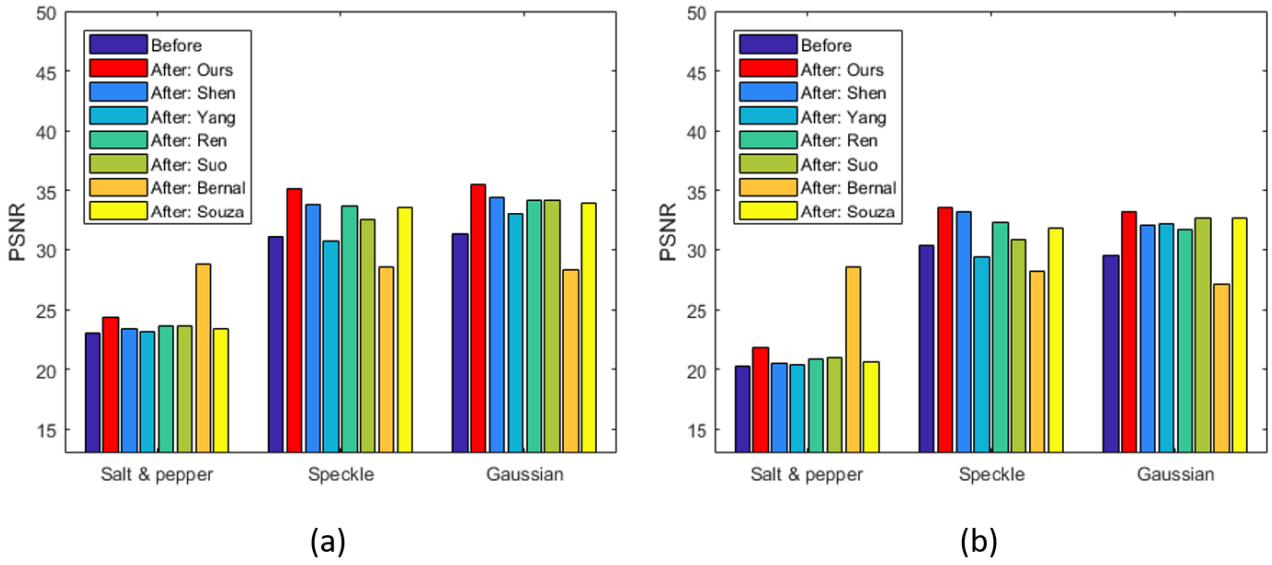

FIGURE 4. Highlight removal performance comparison under noise,(a) noise density = 0.01 for salt and pepper noise, noise variance = 0.01 for speckle noise, and $\sigma = 3$ for Gaussian noise, (b) noise density = 0.02 for salt and pepper noise, noise variance = 0.02 for speckle noise, and $\sigma = 6$ for Gaussian noise.

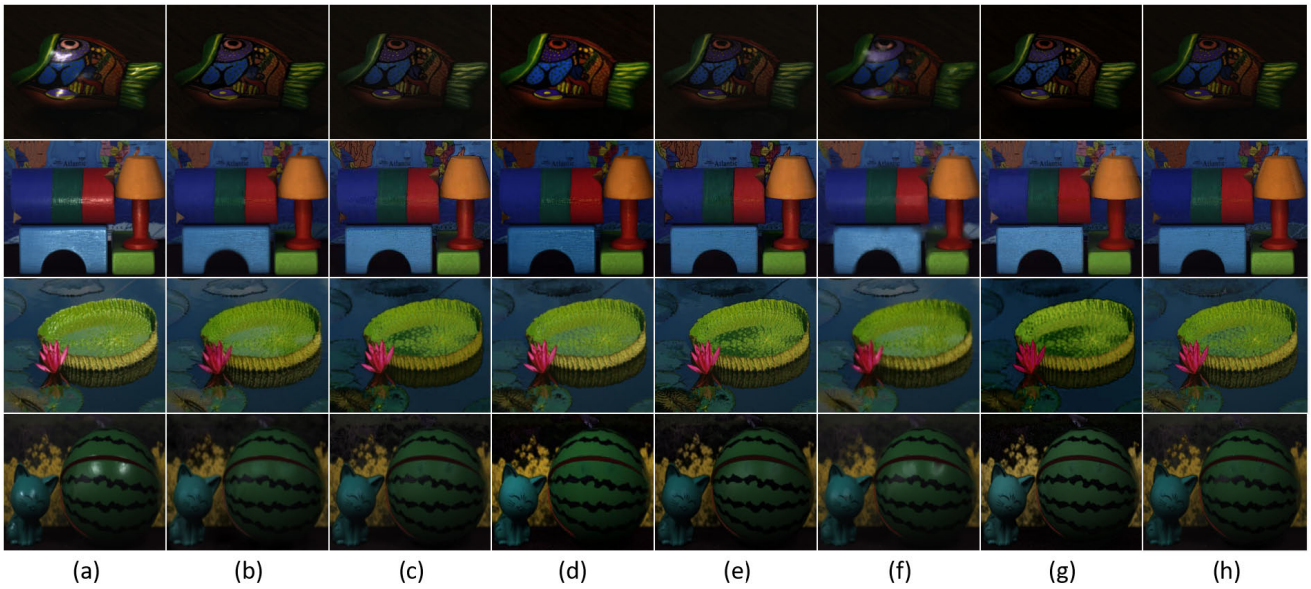

FIGURE 5. Highlight removal results for benchmark natural images: (a) Highlight images, (b) Our method, (c) paper [10], (d) paper [12], (e) paper [11], (f) paper [34],(g) paper [8],(h) paper [45].

Table 2 lists the computed results by the seven methods. We see that the proposed method has competitive performance for highlight removal and structural information preservation, compared with the other six approaches.

To explore the performance of the proposed method in the presence of noise, we performed our method and the other six methods on the four natural images with different types of noise: salt & pepper, speckle, and Gaussian noise, were added. PSNR was used as an evaluation metric. For our evaluation, we take the average PSNR of four images before and after removal of specular reflection. Let salt & pepper noise have noise density of 0.01, speckle noise have variance of 0.01, and Gaussian white noise have a standard deviation of $\sigma = 3$. Fig. 4(a) displays their comparative results. Let salt & pepper noise have noise density of 0.02, speckle noise have variance of 0.02, and Gaussian white noise have a standard deviation of $\sigma = 6$. Fig. 4(b) displays their comparative results. In Figs. 4(a) and 4(b), we see that the proposed method has an improvement in the PSNR of the processed images for speckle and Gaussian noise. On the other hand, the improvement achieved by the proposed method is less than these achieved by Bernal's method due to the use of the median filter during inpainting process.

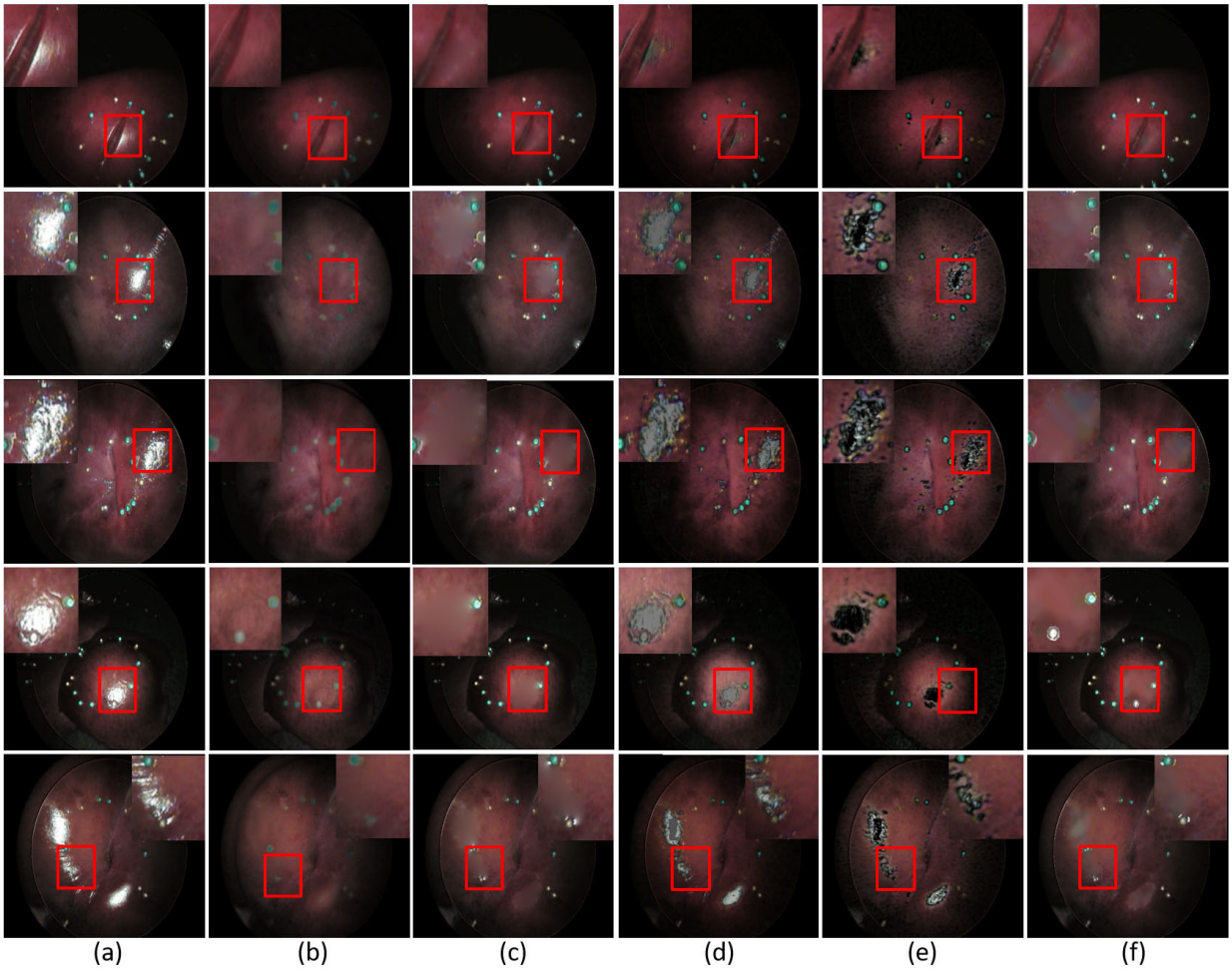

FIGURE 6. Highlight removal results for benchmark endoscopic images: (a) Highlight images, (b) Our method, (c) paper [29], (d) paper [12], (e) paper [11], (f) paper [34].

2) BENCHMARK IMAGE TESTING

We studied four benchmark natural images (Fish, Wood, Lotus, and Watermelon) that have unknown ground truth [10]. Fig. 5 depicts the highlight removal results obtained by the seven methods. In terms of visual inspection, our method produces promising results, which indicates its effectiveness on the natural scenes. Similar to the other five dichromatic reflection model-based methods [8], [10]–[12], [45], our method is comparable in highlight removal, color recovery, and detail preservation. Compared with the inpainting-based method [34], our method maintains the lightness and color fidelity of image background, which is shown in the fish (first row) and the lotus (third row) images in Fig. 5.

B. MEDICAL IMAGE ASSESSMENT

1) BENCHMARK IMAGE TESTING

We studied two groups of benchmark images with saturated highlights and complex textures from the TMI dataset [41]. Fig. 6 demonstrates highlight removal results by five methods on five benchmark images. Highlight removal comparisons are shown in Fig. 6(b)-(f). As shown in Fig. 6(b), our approach removes specular highlights from all endoscopic images and preserves the original texture details and colors on organ surfaces. From local details shown in Fig. 6, it is seen that the other four methods are capable of removing specular highlights, but fail to preserve textures and colors. From Figs. 6(c) and (f), it is seen that Saint-Pierre's [29] and Bernal's methods [34] produce over-smooth images on the highlight regions. From Fig. 6(d) and (e), it is seen that the methods of both Yang *et al.* [11] and Ren *et al.* [12] cause heavy degradation and color distortion.

Fig. 7 depicts highlight removal results of other five benchmark images. Highlight removal comparisons are shown in Fig. 7(b)-(e). In Fig. 7(b), our method removes specular highlights from all endoscopic images and preserves the original texture details and color on organ surfaces. Similarly, from Figs. 7(c) and (f) we see that both Saint-Pierre's and Bernal's methods result in overly smoothed images on the highlight regions. From Figs. 7 (d) and (e), we see that the methods of both Yang *et al.* [11] and Ren *et al.* [12] cause heavy degradation and color distortion.

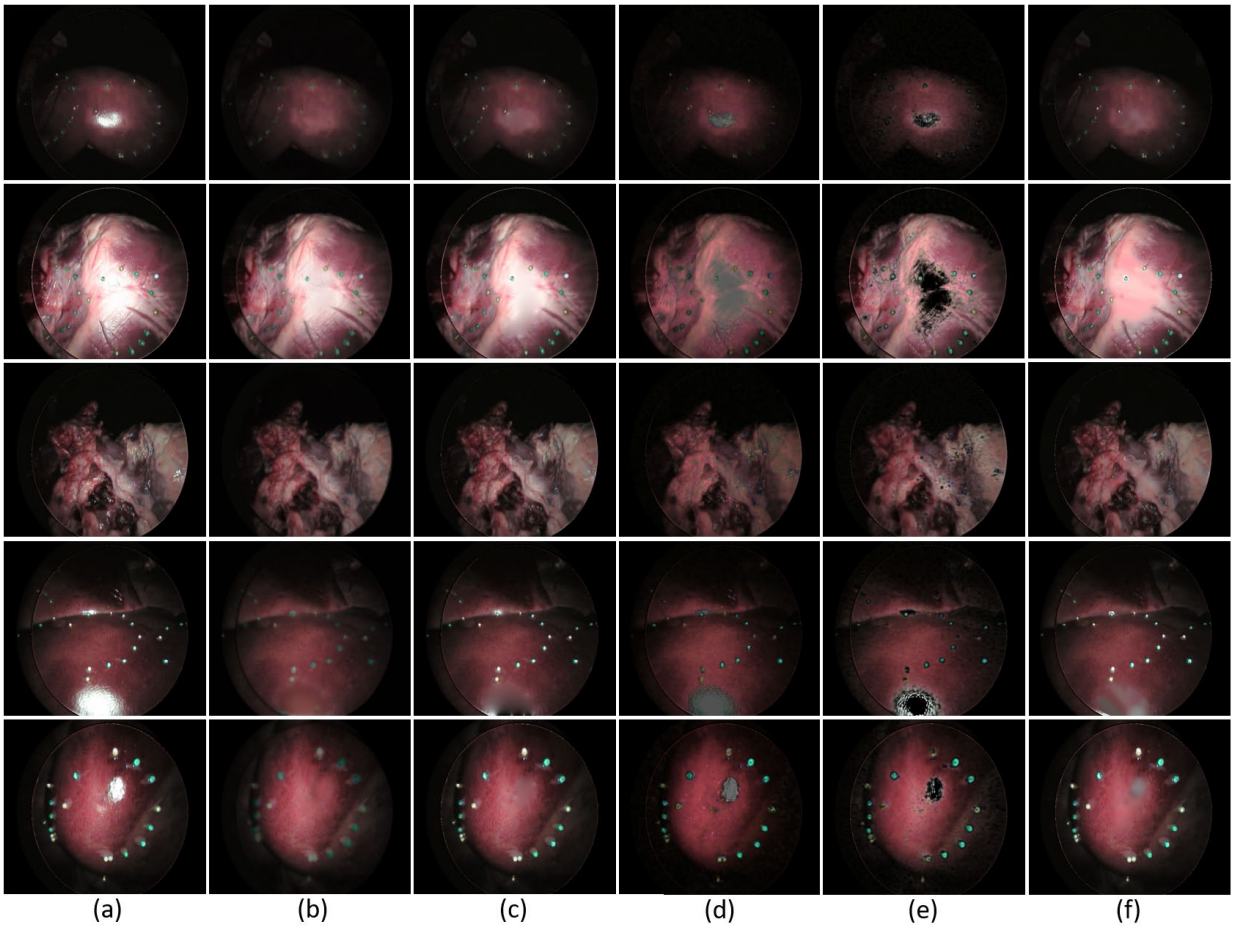

FIGURE 7. Highlight removal results for benchmark endoscopic images: (a) Highlight images, (b) Our method, (c) paper [29], (d) paper [12], (e) paper [11],(f) paper [34].

2) REAL IMAGE TESTING

We studied specular highlight removal from real laparoscopic images with saturated highlights and complex textures acquired from endoscopic surgeries. For our comparison, five real laparoscopic images are shown in Fig. 8(a). Figs. 8(b)-(f) display specular highlight removal results by five methods. It is seen that our method removes specular highlights from all laparoscopic images and preserves original texture details and color on organ surfaces shown in Fig. 8(b). In contrast, the saturated highlight regions are distorted by the methods of Shen and Zheng [10], Yang *et al.* [11], Ren *et al.* [12], and Bernal *et al.* [34], shown in Fig. 8(c), (d), (e), and (f) respectively.

3) FORCED-CHOICE PREFERENCE TESTING

For further quantitative validation, we performed a forced-choice preference experiment on 20 specular highlight images acquired from real 2-D laparoscopic surgeries. Each image was processed by the proposed method and other four highlight removal methods [10]–[12], [34]. Twenty sets of testing images were created, where each set included 5 processed images. Our user study was performed under a protocol approved by the Research Ethics Board of Western University. Twenty clinicians with varying degrees of laparoscopy experience created the test group. The participants included 10 surgeons/fellows with over 5 years of experience and 10 medical residents with less than 5 years of experience. For each trial, two processed images randomly drawn from each image set were shown to the participants, who were blinded to the processing method, and were asked for their preferences. To reduce the number of trials, the previously preferred image remained in the next trial and was paired with an un-compared image from the image set. This process was repeated until all 5 images within the image set were compared and the last remaining preferred image was recorded. The above procedures were repeated for all 20 image sets, and the percentage of each algorithm with the most preferred choice was used as the user's preference score. According to the feedback from the clinical participants, our approach produced the highest score, receiving an average approval rating of 76%, demonstrating significant favor from the participants, while the other four highlight removal methods received less than 24% approval rating.

C. APPLICATION TO STEREO RECONSTRUCTION

The proposed method was applied to stereo reconstruction. We tested our method on 20 benchmark endoscopic images

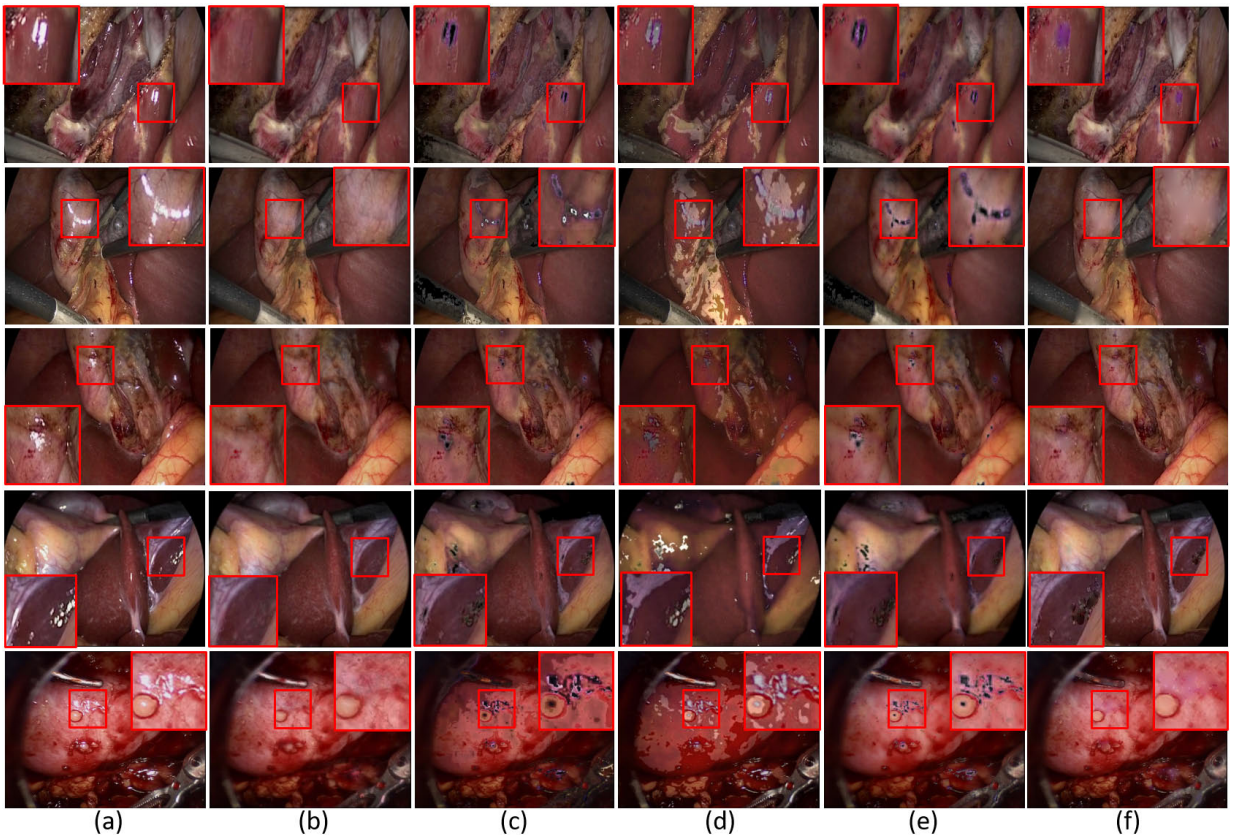

FIGURE 8. Highlight removal results for real laparoscopic images: (a) Highlight images, (b) Our method, (c) paper [10], (d) paper [12], (e) paper [11], (f) paper [34].

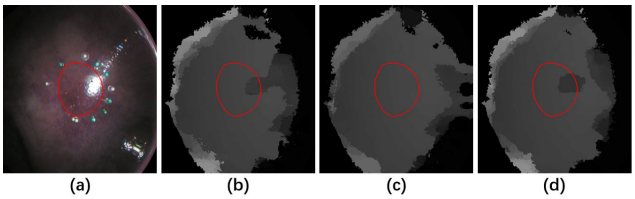

FIGURE 9. Disparity comparison results: (a) Input left highlight image, (b) Disparity map without highlight removal, (c) Disparity map with highlight removal by our algorithm (d) Disparity map with highlight removal by paper [34].

from the ''Distance dataset'' with known ground truth [41]. We performed the cost volume filtering method [40] for stereo reconstruction, based on the unprocessed dataset, the processed dataset by the proposed method, and by the inpainting-based method [34], respectively. The reconstructions based on the proposed method gave the average root mean square distance (RMSD) as 0.69 mm. In contrast, the reconstruction based on [34] yields an RMSD of 1.24 mm, and the unprocessed dataset 1.10 mm. Furthermore, Fig. 9 depicts the comparison of disparity results, where Fig. 9(b) is the disparity map without highlight removal, Fig. 9(c) depicts the result of following our highlight removal approach. Fig. 9(d) is the result of the following inpainting-based method. The red contours of the region of interest indicate that the proposed method gave a smooth disparity map, while others have nonsmooth disparity maps that may lead to inaccurate reconstruction of the 3D surface. It shows that the proposed highlight removal approach has the potential to significantly enhance stereoscopic reconstruction accuracy.

VI. DISCUSSION AND CONCLUSION

This paper proposes a global optimization method for specular highlight removal from a single image, based on the dichromatic reflection model that is widely used in natural images. For effectiveness on medical images, we take advantage of the fact that such images have very small color variation due to the lack of blue and green components, which leads to smooth varying hue in HSV space. We also observe that the saturation layer is smoothly varying, and which doesn't contain any intensity edges in RGB space. Because of these properties, we obtain more accurate hue and saturation estimates using an adaptive inpainting technique. Theoretical analysis shows that estimated diffuse chromaticity can approximate true diffuse chromaticity so that the diffuse refection estimation error can be minimized. Using the estimated diffuse color and modified illumination color, we reformulate the specular highlight removal problem as a convex optimization problem with double regularization. In contrast, current non-convex optimization modeling-based methods for specular highlight removal may suffer from

local minimum problem. Since two regularization terms can describe diffuse and specular component features, the proposed highlight removal method is able to not only remove highlights, but also preserve texture details. The quantitative experimental results demonstrate that the proposed method is effective on benchmark and real endoscopic images as well as natural images, in terms of both image quality and detail preservation, compared with several competing methods. Moreover, forced-choice preference experimental results confirm that the proposed method is accepted by medical experts. Furthermore, having effectively removed highlights from endoscopic images, the proposed method significantly enhances stereo-reconstruction surface accuracy and thus can provide surgeons more accurate depth information for automated surgical guidance.

Because the proposed method combines the detection technique and optimization technique, it has relatively high computational cost. At present, the computational time of our method on our machine is 35 secs for a 600 × 700 benchmark endoscopic image, while the times for the approaches of Ren et al. is 9 secs; Saint-Pierre et al. is 120secs; Bernal et al. is 20 secs, and Yang et al. is 20 secs. Accelerating the proposed method is needed for real-time processing. While the proposed method running in MATLAB is clearly too slow for real-time operation, the procedure is highly parallelizable and amenable to GPU processing. Improvements to optimization procedures could also improve computational efficiency. In addition, temporal information may be helpful for color correction and diffuse chromaticity estimation. Thus, incorporating temporal information can further enhance computational speed and accuracy of the proposed algorithm, and will be the subject of future research.

APPENDIX

PROOF OF PROPOSITION 1

Proof: Substituting $\Gamma_\epsilon(\mathbf{x})$ into (1), we have

$$I(\mathbf{x}) = m_d(\mathbf{x})\Lambda(\mathbf{x}) + m_s(\mathbf{x})\Gamma_\epsilon(\mathbf{x}). \tag{26}$$

Then $I_g(\mathbf{x}) = m_d(\mathbf{x})\Lambda_g(\mathbf{x}) + m_s(\mathbf{x})$, $I_b(\mathbf{x}) = m_d(\mathbf{x})\Lambda_b(\mathbf{x}) + m_s(\mathbf{x})$, and $I_r(\mathbf{x}) = m_d(\mathbf{x})\Lambda_r(\mathbf{x}) + m_s(\mathbf{x})(1-\epsilon)$. If $I(\mathbf{x}) = [1,1,1]^T$ for any $\mathbf{x} \in X_0$, then

$$\begin{cases} 1 - m_s(\mathbf{x})(1-\epsilon) = m_d(\mathbf{x})\Lambda_r(\mathbf{x}) \\ 1 - m_s(\mathbf{x}) = m_d(\mathbf{x})\Lambda_g(\mathbf{x}) \\ 1 - m_s(\mathbf{x}) = m_d(\mathbf{x})\Lambda_b(\mathbf{x}) \end{cases}$$

Thus $m_d(\mathbf{x})max\{\Lambda_r(\mathbf{x}), \Lambda_g(\mathbf{x}), \Lambda_b(\mathbf{x})\} = max\{1 - m_s(\mathbf{x}), 1 - m_s(\mathbf{x})(1-\epsilon)\} = 1 - m_s(\mathbf{x})(1-\epsilon)$. Because $\Lambda_V(\mathbf{x}) = max\{\Lambda_r(\mathbf{x}), \Lambda_g(\mathbf{x}), \Lambda_b(\mathbf{x})\}$, we have $m_d(\mathbf{x})\Lambda_V(\mathbf{x}) = 1 - m_s(\mathbf{x})(1-\epsilon)$. From $\Lambda_V(\mathbf{x}) = 1$ it follows that $m_d(\mathbf{x}) = 1 - m_s(\mathbf{x})(1-\epsilon) > 0$ since $m_s(\mathbf{x})(1-\epsilon) < 1$. If $I(\mathbf{x}) = [1, \eta, \theta]^T$ for any $\mathbf{x} \in X_0$ where $0 \le \eta < 1$ and $0 \le \theta < 1$, then following above analysis we also have for any $\mathbf{x} \in X_0$

$$m_d(\mathbf{x}) = 1 - m_s(\mathbf{x})(1-\epsilon) > 0, \quad \forall \epsilon \in (0,1)$$

since $1 - m_s(\mathbf{x})(1-\epsilon) \ge max\{\eta - m_s(\mathbf{x}), \theta - m_s(\mathbf{x})\}$. □

PROOF OF PROPOSITION 2

Proof: According to the standardized colorimetric transformation [35], we have three Hexcone formulas which convert RGB color space to HSV color space: $V = max\{R,G,B\}$, $S = (V - min\{R,G,B)/V$, and

$$H = \begin{cases} 0, & if\ V = min\{R,G,B\} \\ (60^\circ \times \dfrac{G-B}{V - min\{R,G,B\}} + 360^\circ & \\ mod 360^\circ, & if\ V = R \\ (60^\circ \times \dfrac{G-B}{V - min\{R,G,B\}} + 360^\circ), & if\ V = G \\ (60^\circ \times \dfrac{G-B}{V - min\{R,G,B\}} + 240^\circ), & if\ V = B \end{cases} \tag{27}$$

It is seen that $kV = max\{kR, kG, kB\}$ and $(kV - min\{kR, kG, kB\})/(kV) = k(V - min\{R,G,B\})/(kV) = S$. Again from (27) we have

$$\frac{(kG - kB)}{kV - min\{kR, kG, kB\}} = \frac{(G-B)}{(V - min\{R,G,B\})}.$$

Thus (27) still holds for any (kR, kG, kB) and kV. It follows (20). □

PROOF OF PROPOSITION 3

Proof: According to Proposition 2 we see for any free color pixel $\mu > 0$

$$\varphi(\mu R, \mu G, \mu B) = (H, S, \mu V) \tag{28}$$

Then $\mu(R,G,B) = \varphi^{-1}(H, S, \mu V)$ and thus

$$(R,G,B) = \{\varphi^{-1}(H, S, \mu V)\}/\mu \tag{29}$$

Let $\mu = 1/V$. Then

$$(R,G,B) = V\varphi^{-1}(H, S, 1) \tag{30}$$

On the other side, we have

$$(R,G,B) = \varphi^{-1}(H, S, V) \tag{31}$$

From both (30) and (31) it follows (21). □

PROOF OF THEOREM 1

Proof: Let the diffuse reflection vector be

$$I_D(\mathbf{x}) = (I_{Dr}, I_{Dg}, I_{Db}) = m_d(\mathbf{x})\Lambda(\mathbf{x}). \tag{32}$$

Using HSV transformation we have

$$\varphi(I_{Dr}, I_{Dg}, I_{Db}) = (I_{DH}, I_{DS}, I_{DV}) \tag{33}$$

By Proposition 3 we know that $\varphi^{-1}(I_{DH}, I_{DS}, 1) = \{\varphi^{-1}(I_{DH}, I_{DS}, I_{DV})\}/I_{DV}$. Then

$$\varphi^{-1}(I_H^*, I_S^*, 1) \approx \{\varphi^{-1}(I_{DH}, I_{DS}, I_{DV})\}/I_{DV}.$$

Note that $\varphi^{-1}(I_{DH}, I_{DS}, I_{DV}) = \varphi^{-1}(\varphi(I_{Dr}, I_{Dg}, I_{Db})) = (I_{Dr}, I_{Dg}, I_{Db})$. Then

$$\varphi^{-1}(I_H^*, I_S^*, 1) \approx (I_{Dr}, I_{Dg}, I_{Db})/I_{DV}.$$

By using $\Lambda^*(\mathbf{x}) = \varphi^{-1}(I_H^*, I_S^*, 1)$ and (32), we obtain that

$$I_{DV}\Lambda^*(\mathbf{x}) \approx (I_{Dr}, I_{Dg}, I_{Db}) = m_d(\mathbf{x})\Lambda(\mathbf{x}).$$

On the other side, because $I_D(\mathbf{x})$ and $I_S(\mathbf{x})$ are nonnegative, $0 \leq I(\mathbf{x}) \leq 1$ implies that $0 \leq I_D(\mathbf{x}) \leq 1$. That is, $0 \leq I_{Dr}, I_{Dg}, I_{Db} \leq 1$. Note that $I_{DV} = max\{I_{Dr}, I_{Dg}, I_{Db}\}$. Then $0 \leq I_{DV} \leq 1$. □

PROOF OF THEOREM 2

Proof: Note that $\mathbf{y}^T\mathbf{y}/2 = \max_{\mathbf{q}}\{\mathbf{q}^T\mathbf{y} - \mathbf{q}^T\mathbf{q}/2\}$ and $||\mathbf{y}||_1 = \max_{||\mathbf{p}||_\infty \leq 1}\{\mathbf{p}^T\mathbf{y}\}$ for any vector $\mathbf{y} \in R^2$ where $||\mathbf{p}||_\infty = max\{|p_1|, |p_2|\}$. (18) is thus rewritten as:

$$\begin{aligned} &E_2(m_d(\mathbf{x}), m_s(\mathbf{x})) \\ &\quad = \max_{\mathbf{p},\mathbf{q}} \beta_1(\mathbf{q}^T\nabla m_d(\mathbf{x}) - ||\mathbf{q}||_2^2/2) + \beta_2\mathbf{p}^T\nabla m_s(\mathbf{x}) \end{aligned} \tag{34}$$

where $\mathbf{q}, \mathbf{p} \in R^2$ and $||p||_\infty \leq 1$. Let

$$\begin{aligned} &E(m_d(\mathbf{x}), m_s(\mathbf{x}), \mathbf{p}, \mathbf{q}) \\ &\quad = E_1(m_d(\mathbf{x}), m_s(\mathbf{x})) + \beta_1\mathbf{q}^T\nabla m_d(\mathbf{x}) - \beta_1||\mathbf{q}||_2^2/2 \\ &\qquad + \beta_2\mathbf{p}^T\nabla m_s(\mathbf{x}) \end{aligned} \tag{35}$$

where Ω_1, Ω_2, and Ω_3 are defined in (23). Then solving (19) is equivalent to solving:

$$\begin{aligned} &\min_{m_d, m_s} \max_{\mathbf{p},\mathbf{q}} E(m_d(\mathbf{x}), m_s(\mathbf{x}), \mathbf{p}(\mathbf{x}), \mathbf{q}(\mathbf{x})) \\ &s.t.\ (m_d(\mathbf{x}), m_s(\mathbf{x})) \in \Omega_1 \times \Omega_2 \\ &\qquad (\mathbf{p}(\mathbf{x}), \mathbf{q}(\mathbf{x})) \in \Omega_3 \times R^2. \end{aligned} \tag{36}$$

According to the saddle point theorem [38], $(m_d^*, m_s^*, \mathbf{p}^*, \mathbf{q}^*)$ is a global minimum point of (36) if and only if for any $(m_d, m_s, \mathbf{p}, \mathbf{q}) \in \Omega_1 \times \Omega_2 \times \Omega_3 \times R^2$

$$E(m_d^*, m_s^*, \mathbf{p}, \mathbf{q}) \leq E(m_d^*, m_s^*, \mathbf{p}^*, \mathbf{q}^*) \leq E(m_d, m_s, \mathbf{p}^*, \mathbf{q}^*). \tag{37}$$

From the right inequality of (37), (m_d^*, m_s^*) is a minimum point of $E(m_d, m_s, \mathbf{p}^*, \mathbf{q}^*)$. From [39] it follows that (m_d^*, m_s^*) satisfies:

$$(m_d - m_d^*)\frac{\partial E}{\partial m_d} \geq 0, \quad \forall m_d \in \Omega_1. \tag{38}$$

and

$$(m_s - m_s^*)\frac{\partial E}{\partial m_s} \geq 0, \quad \forall m_s \in \Omega_2. \tag{39}$$

Similarly, from the left inequality of (38), we see that $(\mathbf{p}^*, \mathbf{q}^*)$ is a minimum point of $E(m_d^*, m_s^*, \mathbf{p}, \mathbf{q})$. It follows that

$$(\mathbf{p} - \mathbf{p}*)^T\frac{\partial E}{\partial \mathbf{p}} \geq 0, \quad \forall \mathbf{p} \in \Omega_3 \tag{40}$$

and

$$(\mathbf{q} - \mathbf{q}^*)^T\frac{\partial E}{\partial \mathbf{q}} \geq 0, \quad \forall \mathbf{q} \in R^2. \tag{41}$$

According to the projection Theorem [39], (38) equals $m_d(\mathbf{x}) = P_{\Omega_1}[m_d(\mathbf{x}) - \frac{\partial E}{\partial m_d}]$, (39) equals $m_s(\mathbf{x}) = P_{\Omega_2}[m_s(\mathbf{x}) - \frac{\partial E}{\partial m_s}]$, (40) equals $\mathbf{p}(\mathbf{x}) = P_{\Omega_3}[\mathbf{p}(\mathbf{x}) - \frac{\partial E}{\partial \mathbf{p}}]$, and (41) equals $\frac{\partial E}{\partial \mathbf{q}} = 0$. □

ACKNOWLEDGMENTS

The authors would like to thank the associate editor and reviewers for their encouragement and valued comments. The authors would also like to thank Dr. John S.H. Baxter and Dr. Jonathan McLeod for the valuable discussions and thank Jackie Williams for paper editing.

REFERENCES

[1] D. A. Ross, J. Lim, R.-S. Lin, and M.-H. Yang, "Incremental learning for robust visual tracking," *Int. J. Comput. Vis.*, vol. 77, nos. 1–3, pp. 125–141, 2008.

[2] A. Artusi, F. Banterle, and D. Chetverikov, "A survey of specularity removal methods," *Comput. Graph. Forum*, vol. 30, no. 8, pp. 2208–2230, 2011.

[3] C. Nezhat, F. Nezhat, and C. Nezhat, *Nezhat's Video-Assisted and Robotic-Assisted Laparoscopy and Hysteroscopy with DVD*. Cambridge, U.K.: Cambridge Univ. Press, 2013.

[4] X. Luo, K. Mori, and T. M. Peters, "Advanced endoscopic navigation: Surgical big data, methodology, and applications," *Annu. Rev. Biomed. Eng.*, vol. 20, no. 1, pp. 221–251, 2018.

[5] M. W. Tao, J.-C. Su, T.-C. Wang, J. Malik, and R. Ramamoorthi, "Depth estimation and specular removal for glossy surfaces using point and line consistency with light-field cameras," *IEEE Trans. Pattern Anal. Mach. Intell.*, vol. 38, no. 6, pp. 1155–1169, Jun. 2016.

[6] B. Münzer, K. Schoeffmann, and L. Böszörmenyi, "Content-based processing and analysis of endoscopic images and videos: A survey," *Multimedia Tools Appl.*, vol. 77, no. 1, pp. 1323–1362, 2018.

[7] J. S. H. Baxter, M. Rajchl, A. J. McLeod, J. Yuan, and T. M. Peters, "Directed acyclic graph continuous max-flow image segmentation for unconstrained label orderings," *Int. J. Comput. Vis.*, vol. 123, no. 3, pp. 415–434, 2017.

[8] J. Suo, D. An, X. Ji, H. Wang, and Q. Dai, "Fast and high quality highlight removal from a single image," *IEEE Trans. Image Process.*, vol. 25, no. 11, pp. 5441–5454, Nov. 2016.

[9] S. A. Shafer, "Using color to separate reflection components," *Color Res. Appl.*, vol. 10, no. 4, pp. 210–218, 1985.

[10] H.-L. Shen and Z.-H. Zheng, "Real-time highlight removal using intensity ratio," *Appl. Opt.*, vol. 52, no. 19, pp. 4483–4493, Jul. 2013.

[11] Q. Yang, J. Tang, and N. Ahuja, "Efficient and robust specular highlight removal," *IEEE Trans. Pattern Anal. Mach. Intell.*, vol. 37, no. 6, pp. 1304–1311, Jun. 2015.

[12] W. Ren, J. Tian, and Y. Tang, "Specular reflection separation with color-lines constraint," *IEEE Trans. Image Process.*, vol. 26, no. 5, pp. 2327–2337, May 2017.

[13] R. T. Tan, K. Nishino, and K. Ikeuchi, "Separating reflection components based on chromaticity and noise analysis," *IEEE Trans. Pattern Anal. Mach. Intell.*, vol. 26, no. 10, pp. 1373–1379, Oct. 2004.

[14] R. T. Tan and K. Ikeuchi, "Separating reflection components of textured surfaces using a single image," *IEEE Trans. Pattern Anal. Mach. Intell.*, vol. 27, no. 2, pp. 178–193, Feb. 2005.

[15] H.-L. Shen and Q.-Y. Cai, "Simple and efficient method for specularity removal in an image," *Appl. Opt.*, vol. 48, no. 14, pp. 2711–2719, 2009.

[16] J. Yang, L. Liu, and S. Z. Li, "Separating specular and diffuse reflection components in the HSI color space," in *Proc. IEEE Int. Conf. Comput. Vis. Workshops*, Jun. 2013, pp. 891–898.

[17] S. M. Z. A. Shah, S. Marshall, and P. Murray, "Removal of specular reflections from image sequences using feature correspondences," *Mach. Vis. Appl.*, vol. 28, nos. 3–4, pp. 409–420, 2017.

[18] X. Wei, X. Xu, J. Zhang, and Y. Gong, "Specular highlight reduction with known surface geometry," *Comput. Vis. Image Understand.*, vol. 168, pp. 132–144, Mar. 2018.

[19] T. Nguyen, Q. N. Vo, H.-J. Yang, S.-H. Kim, and G.-S. Lee, "Separation of specular and diffuse components using tensor voting in color images," *Appl. Opt.*, vol. 53, no. 33, pp. 7924–7936, 2014.

[20] Y. Zhao, Q. Peng, J. Xue, and S. G. Kong, "Specular reflection removal using local structural similarity and chromaticity consistency," in *Proc. IEEE Int. Conf. Image Process. (ICIP)*, Sep. 2015, pp. 3397–3401.

[21] H. Kim, H. Jin, S. Hadap, and I. Kweon, "Specular reflection separation using dark channel prior," in *Proc. IEEE Conf. Comput. Vis. Pattern Recognit. (CVPR)*, Jun. 2013, pp. 1460–1467.

[22] F. Wang, S. Ainouz, C. Petitjean, and A. Bensrhair, "Polarization-based specularity removal method with global energy minimization," in *Proc. IEEE Int. Conf. Image Process. (ICIP)*, Sep. 2016, pp. 1983–1987.
[23] Q. Yang, S. Wang, N. Ahuja, and R. Yang, "A uniform framework for estimating illumination chromaticity, correspondence, and specular reflection," *IEEE Trans. Image Process.*, vol. 20, no. 1, pp. 53–63, Jan. 2011.
[24] P. Tan, S. Lin, L. Quan, and H.-Y. Shum, "Highlight removal by illumination-constrained inpainting," in *Proc. 9th IEEE Int. Conf. Comput. Vis. (ICCV)*, Oct. 2003, pp. 164–169.
[25] F. Ortiz and F. Torres, "A new inpainting method for highlights elimination by colour morphology," in *Proc. Int. Conf. Pattern Recognit. Image Anal.*, 2005, pp. 368–376.
[26] T. Stehle, "Removal of specular reflections in endoscopic images," *Acta Polytechnica, J. Adv. Eng.*, vol. 46, no. 4, pp. 32–36, 2006.
[27] M. Arnold, A. Ghosh, S. Ameling, and G. Lacey, "Automatic segmentation and inpainting of specular highlights for endoscopic imaging," *EURASIP J. Image Video Process.*, vol. 2010, Dec. 2010, Art. no. 814319.
[28] O. Meslouhi, M. Kardouchi, H. Allali, T. Gadi, and Y. Benkaddour, "Automatic detection and inpainting of specular reflections for colposcopic images," *Open Comput. Sci.*, vol. 1, no. 3, pp. 341–354, 2011.
[29] C.-A. Saint-Pierre, J. Boisvert, G. Grimard, and F. Cheriet, "Detection and correction of specular reflections for automatic surgical tool segmentation in thoracoscopic images," *Mach. Vis. Appl.*, vol. 22, no. 1, pp. 171–180, Jan. 2011.
[30] S.-T. Lee, T.-H. Yoon, K.-S. Kim, K.-D. Kim, and W. Park, "Removal of specular reflections in tooth color image by perceptron neural nets," in *Proc. 2nd Int. Conf. Signal Process. Syst.*, Jul. 2010, pp. V1-285–V1-289.
[31] A. Morgand and M. Tamaazousti, "Generic and real-time detection of specular reflections in images," in *Proc. Int. Conf. Comput. Vis. Theory Appl. (VISAPP)*, Jan. 2014, pp. 274–282.
[32] I. Funke, S. Bodenstedt, C. Riediger, J. Weitz, and S. Speidel, "Generative adversarial networks for specular highlight removal in endoscopic images," *Proc. SPIE*, vol. 10576, Mar. 2018, Art. no. 1057604.
[33] J. Oh, S. Hwang, J. Lee, W. Tavanapong, J. Wong, and P. C. de Groen, "Informative frame classification for endoscopy video," *Med. Image Anal.*, vol. 11, no. 2, pp. 110–127, Apr. 2007.
[34] J. Bernal, J. Sánchez, and F. Vilariño, "Impact of image preprocessing methods on polyp localization in colonoscopy frames," in *Proc. 35th Annu. Int. Conf. IEEE Eng. Med. Biol. Soc. (EMBC)*, Jul. 2013, pp. 7350–7354.
[35] A. R. Smith, "Color gamut transform pairs," in *Proc. 5th Annu. Conf. Comput. Graph. Interact. Techn. (SIGGRAPH)*, 1978, pp. 12–19.
[36] J.-F. Aujol, G. Gilboa, T. Chan, and S. Osher, "Structure-texture image decomposition—Modeling, algorithms, and parameter selection," *Int. J. Comput. Vis.*, vol. 67, no. 1, pp. 111–136, 2006.
[37] H. Schaeffer and S. Osher, "A low patch-rank interpretation of texture," *SIAM J. Imag. Sci.*, vol. 6, no. 1, pp. 226–262, 2013.
[38] S. Boyd and L. Vandenberghe, *Convex Optimization*. Cambridge, U.K.: Cambridge Univ. Press, 2015.
[39] D. Kinderlehrer and G. Stampacchia, *An Introduction to Variational Inequalities and Their Applications*. New York, NY, USA: Academic, 1980.
[40] A. Hosni, C. Rhemann, M. Bleyer, C. Rother, and M. Gelautz, "Fast cost-volume filtering for visual correspondence and beyond," *IEEE Trans. Pattern Anal. Mach. Intell.*, vol. 35, no. 2, pp. 504–511, Feb. 2013.
[41] L. Maier-Hein *et al.*, "Comparative validation of single-shot optical techniques for laparoscopic 3-D surface reconstruction," *IEEE Trans. Med. Imag.*, vol. 33, no. 10, pp. 1913–1930, Oct. 2014.
[42] Y. Akashi and T. Okatani, "Separation of reflection components by sparse non-negative matrix factorization," *Comput. Vis. Image Understand.*, vol. 146, pp. 77–85, May 2016.
[43] C. Li, S. Lin, K. Zhou, and K. Ikeuchi, "Specular highlight removal in facial images," in *Proc. IEEE Conf. Comput. Vis. Pattern Recognit. (CVPR)*, 2017, pp. 3107–3116.
[44] S. Wang, C. Yu, Y. Sun, F. Gao, and J. Dong, "Specular reflection removal of ocean surface remote sensing images from UAVs," *Multimedia Tools Appl.*, vol. 77, no. 9, pp. 11363–11379, 2018.
[45] A. C. dos Santos Souza, M. C. de Farias Macedo, V. P. do Nascimento, and B. S. Oliveira, "Real-time high-quality specular highlight removal using efficient pixel clustering," in *Proc. 31st SIBGRAPI Conf. Graph., Patterns Images (SIBGRAPI)*, Parana, Brazil, Oct./Nov. 2018, pp. 56–63.
[46] J. Guo, Z. Zhou, and L. Wang, "Single image highlight removal with a sparse and low-rank reflection model," in *Computer Vision—ECCV* (Lecture Notes in Computer Science), 2018, pp. 282–298.
[47] J. Khan, A. S. Malik, N. Kamel, and S. C. Dass, "Highlights removal using reflected energy and histogram analysis," *J. Eng. Res.*, vol. 7, no. 1, pp. 1–13, 2019.

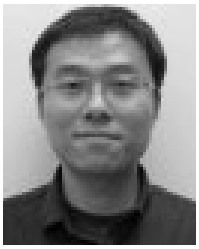

WENYAO XIA received the bachelor's degree in engineering science and the master's degree in electrical and computer engineering from the University of Toronto, in 2011 and 2013, respectively. He is currently pursuing the Ph.D. degree in medical biophysics with Western University. His current research interests include image enhancement, stereo matching, deep learning, and their applications in medical images.

ELVIS C. S. CHEN received the Ph.D. degree from the School of Computing, Queen's University, Canada, in 2007. He is currently a Scientist with Robarts Research Institute, with cross appointments to Western University, Canada. He is working in the field of computer-assisted surgery, his research goal is to assist surgeons in their surgical delivery by devising novel computerized surgical workflow. His research interests include surgical metrology, visualization and perception, medical robotics, and mixed reality environments.

STEPHEN E. PAUTLER graduated from the Medical School, University of Calgary, in 1995, and subsequently completed the urology residency at Western University. He is currently an Associate Professor with the Departments of Surgery and Oncology. His research interests include the application of minimally invasive surgical techniques and image-guided ablative procedures for urologic cancers.

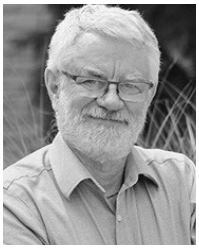

TERRY M. PETERS received the Ph.D. degree in electrical engineering from University of Canterbury, in 1973. He is currently a Professor of medical biophysics with Western University and a Scientist with Robarts Research Institute. His research interests include image-guided surgery, 3-D visualization, instrument tracking, multimodality image registration, cardiac imaging, stereoscopic visualization, and virtual reality.